



Innovative strategy of turning waste into treasure: High-efficiency adsorption of heavy metals pollutants by modified amorphous calcium phosphate prepared with phosphogypsum waste

Zhiren Zhao, Zhongtian Dong, Fenghe Wang, Fengyun Wang, Mingzhu Xia*

School of Chemistry and Chemical Engineering, Nanjing University of Science and Technology, Nanjing 210094, China

ARTICLE INFO

Keywords:

Phosphogypsum
Amorphous calcium phosphate
Heavy metal ions
Adsorption
Mechanism

ABSTRACT

In the present work, phosphogypsum (PG) waste was used as a calcium source, and integrated with 2-hydroxyphosphonoacetic acid (HPA) doping, modified inorganic-organic amorphous calcium phosphate hybrid composite was prepared, to remove Cd²⁺ and Co²⁺ in aqueous solution. The study demonstrated that when pH=8, the equilibrium adsorption capacity of hydroxyapatite (HAP) for Cd²⁺ and Co²⁺ can reach 275.84 mg/g and 70.63 mg/g, respectively. After modification with HPA, the adsorption capacity of 20HPA-HAP for Cd²⁺ and Co²⁺ was higher at 468.92 mg/g and 171.38 mg/g, respectively. Regeneration experiments show that the adsorbent has good recycling performance, and the adsorbent has a good adsorption effect on low-concentration cadmium and cobalt ions in the actual hard gold electroplating wastewater. Meanwhile, the adsorption mechanism of 20HPA-HAP for Cd²⁺ and Co²⁺ was vividly visualized through Multiwfnn wavefunction program and VMD program. Therefore, the reason why doping HPA greatly improves the adsorption performance of amorphous calcium phosphate on heavy metal ions was revealed from the atomic point of view. The findings suggest a promising approach for the effective utilization of discarded PG and the effective treatment of heavy metal pollution in industrial wastewater, highlighting the dual benefit of waste material repurposing and pollution control, which was an innovative strategy of turning waste into treasure.

1. Introduction

The discharge of wastewater, exhaust gases, and waste residues in some industrial processes related to heavy metals is the main source of heavy metal pollution. Among them, cobalt ions can cause chronic poisoning, causing damage to organs such as the lungs, heart, thyroid, and kidneys. Cadmium poisoning can cause a range of health problems, including kidney damage, bone disease, liver damage, and an increased risk of cancer. Therefore, given the priority placed on ecological conservation and the assurance of food safety, the imperative of efficiently eliminating heavy metal ions from wastewater is becoming more conspicuous [1–3].

In contrast to chemical, biological, and alternative physical approaches used to eliminate heavy metal ions, adsorption stands out as an effective, cost-effective, and eco-friendly technique [4–9]. Many inexpensive adsorbents have been exploited for adsorptive removal of different pollutants [10–12]. Hong et al. [13] prepared low-cost adsorbents from paper industry waste (newspaper (NP) and white paper (WP)

waste) and used them to remove Pb(II), the maximum adsorption capacity was 42.4 and 18.5 mg/g, respectively according to Langmuir isotherm model. Edgar P.P et al. [14] prepared biochar from agricultural by-products to adsorb Pb²⁺ and Cd²⁺ from drinking water, and the removal efficiency can reach 95.96% for Pb²⁺ and 99.05% for Cd²⁺. He et al. [15] reported the low-cost carboxymethyl chitosan-kaolinite composite hydrogel to remove Cu²⁺, and the maximum adsorption capacities for Cu²⁺ can reach 206 mg/g.

Among the many sorbents, hydroxyapatite (HAP) has a wide range of applications in the field of pollutant adsorption treatment because of its versatile, non-toxic, chemical stability, cost-effectiveness, biocompatibility, and good adsorption performance for heavy metals [16–24]. To further improve the adsorption performance of HAP, a large number of HAP-modified composites have been explored and reported. Wang et al. [25] fabricated hydroxyapatite-biochar nanocomposite with the advantages of both biochar and hydroxyapatite nanoparticles for removing Pb(II), Cu(II), and Zn(II). Guo et al. [26] obtained bitter gourd-shaped nano HAP by the addition of mono-dodecyl phosphate potassium, the

* Corresponding author.

E-mail address: xiamzh196808@njust.edu.cn (M. Xia).

adsorption capacity is 815 mg/g for Pb^{2+} , 291 mg/g for Cd^{2+} and 187 mg/g for Cr^{3+} , respectively. Qurat U. A. et al. [27] prepared a hydroxyapatite-magnetite-bentonite composite for efficient adsorption of $\text{Pb}(\text{II})$, $\text{Cd}(\text{II})$, and crystal violet from aqueous solution, and the adsorption capacity for $\text{Pb}(\text{II})$ (482 mg/g) and $\text{Cd}(\text{II})$ (309 mg/g) can be obtained.

Common synthetic methods of HAP and its composites include wet chemical precipitation, hydrothermal method, sol-gel method, and ultrasonic and microwave-assisted methods [28]. Co-precipitation is the most commonly used method for preparing hydroxyapatite due to its simplicity and mild reaction conditions [29–31]. Phosphorus source and calcium source are the precursors of HAP synthesis. Commonly used phosphorus sources include ammonium dihydrogen phosphate, diammonium hydrogen phosphate, orthophosphate, etc. Calcium sources can be selected calcium hydroxide, calcium chloride, and calcium nitrate. How to utilize calcium-containing waste materials as a source of calcium is one of the key factors in reducing the production and usage costs of hydroxyapatite.

Phosphogypsum (PG) constitutes an industrial byproduct generated in the course of phosphoric acid and phosphate fertilizer production through a wet method. For each ton of P_2O_5 produced, the quantity of PG waste typically ranges from 4.5 to 5.5 tons [32–34]. The annual accumulation rate of approximately 300 million metric tons (Mton) of PG, and only a limited number of quantities employed across various application domains (approximately 15%) [35]. The majority of PG is managed through open-air stacking, which not only occupies a significant amount of land resources but also causes pollution to the atmosphere, water systems, and soil due to wind and rain erosion [35]. Therefore, there is a growing need to explore approaches for environmentally sustainable and cost-effective utilization of existing PG stockpiles. Utilizing PG as the source of calcium in the production of nano-hydroxyapatite (nHAP) offers the potential to establish an effective waste management solution while also making use of an economically advantageous raw material, the byproduct ammonium sulfate can also be used as a fertilizer. Only a few literature have reported the preparation of HAP by PG as an adsorbent for lead ions, fluorine ions, and dye [32,34,36–38]. In addition to the common chemical precipitation method, Hiba Bensalah et al. [39] prepared the nanocrystalline HAP material with PG waste as a calcium source by hydrothermal method.

Organic phosphonates are commonly used as corrosion inhibitors and scale inhibitors, in limited literature, they have been used to incorporate HAP to prepare inorganic-organic hybrid HAP composites [40–44]. Due to the strong affinity between organo-phosphonates and HAP, phosphonates doped in the preparation of HAP will affect the crystallinity and surface properties of HAP, and thus affect the adsorption performance. On the other hand, there is strong complexation between organo-phosphonates and many metal ions, the adsorption capacity of HAP composites modified by organic phosphonates was much higher than that of unmodified HAP [40–44]. Yasmine Daniels S. et al. [41] found that the incorporation of 1-hydroxyethane-1,1-diphosphonic acid (HEDP) into HAP can greatly improve the affinity for heavy metal ions in aqueous solution, with an affinity sequence of $\text{Pb}(\text{II}) > \text{Cd}(\text{II}) > \text{Zn}(\text{II}) > \text{Ni}(\text{II}) > \text{Cu}(\text{II})$. Saoiabi et al. [40] grafted HAP with amino-trimethylphosphonic acid (ATMP) and found that the maximum adsorption capacities of modified HAP were 454 mg/g (Pb^{2+}) and 270 mg/g (Zn^{2+}), respectively, which were twice of unmodified HAP. In our previous work [43], the adsorption capacity of diethylenetriaminepenta (methylene phosphonic) acid (DTPMP)-doped hydroxyapatite for Pb^{2+} was more than 10 times that of purchased commercial HAP nanopowder. In another work [44], the adsorption capacity of amino trimethylphosphate (ATMP) functionalized hydroxyapatite for Pb^{2+} and Cd^{2+} was 1.76 times and 1.90 times that of undoped HAP.

2-Hydroxyphosphonoacetic acid (HPA) is a molecule that contains phosphonyl, carboxyl, and hydroxyl functional groups, which gives it an effective chelating agent for various metal ions [45]. It has excellent

chemical stability, is resistant to hydrolysis, and is not easily degraded by acid or alkali. Similar to DTPMP and ATMP, it is widely employed as a scale and corrosion inhibitor in recirculating cooling water systems in industries such as steel, petrochemicals, power generation, and pharmaceuticals [46–48]. In limited literature reports on the application of HPA, researchers have used the complex properties of HPA with various metal ions to study its corrosion inhibition properties to steel or to prepare metal ion-HPA complexes. Lin et al. [48] prepared polyaniline (PANI)/HPA/ ZrO_2 /epoxy (EP) composite coating to be the metal protection coating in the marine environment, the chelation of HPA with iron ions enhanced the corrosion inhibition of steel, giving the coating superior anti-corrosion properties. Dong et al. [49] prepared novel 3D cadmium phosphonate with double-stranded helical channels by the complexation of HPA with Cd. In addition, Yang et al. [50] utilized HPA's good complexation with metal ions and selected HPA as the mixed linker and surface modifier to prepare the phosphoric acid functionalized defective UiO-66-NH₂, to be the effective adsorbent of rare earth metal ion Gd(III). The results illustrated that the phosphate groups of HPA molecule and Zr-O clusters contributed to the Gd(III) adsorption on defective UiO-66-NH₂-supported ion imprinted polymers, and displayed a high adsorption capacity of 181.75 mg/g and a short equilibration time of 30 min for Gd(III). Except this, as far as we know, no other reports have found that HPA has been used as a modifier to prepare adsorbent composites. Moreover, in the limited reports on the modification of HAP by organo-phosphonates, calcium hydroxide [40, 41] or calcium chloride [42,43] was used as the calcium source of HAP, and no PG waste was used as the calcium source.

Therefore, in the present work, we applied waste PG as a calcium source, phosphoric acid as an inorganic phosphorus source, and HPA as a dopant to provide an organophosphorus source to prepare inorganic-organic hybrid nano-hydroxyapatite, to be the efficient adsorbent of heavy metal ions (Cd^{2+} and Co^{2+}). This endeavor not only addresses the pollution issue associated with waste PG but also culminates in the creation of an organic-inorganic hybrid adsorbent boasting exceptional capabilities in adsorbing heavy metals. The by-product ammonium sulfate can also be applied as a synthetic fertilizer specifically tailored for alkaline soils.

2. Materials and methods

2.1. Materials

PG and H_3PO_4 (85%) were obtained from the Guizhou Phosphating Group. $\text{Co}(\text{NO}_3)_2$ and $\text{Cd}(\text{NO}_3)_2$ and all others were procured from Aladdin (located in Shanghai, China), while HPA (with an active content of 50%) was supplied by Xintai Water Treatment Co. Ltd (based in Zaozhuang, Shandong, China).

2.2. The structural characteristics of dopant HPA

The structural formula of dopant HPA is displayed in Fig. 1(a), the same carbon atom is connected with a phosphonic acid group, a hydroxyl group, and a carboxyl group. Gaussian 09 [51] with a B3LYP /6–311 G* was utilized to optimize the structure of HPA, and then visualized through Multifwn wavefunction program and VMD program [52] (Fig. 1(b–d)). In Fig. 1(b), there is a dark blue isosurface between a phosphonic acid hydrogen atom and the carboxyl oxygen atom, indicating that there is strong intramolecular hydrogen bonding between the phosphonic acid O atom and carboxyl O atom. Meanwhile, the green slab between the phosphonic acid O atom and the hydroxyl H atom implied the weak intramolecular hydrogen bonding between the phosphonic acid O atom and hydroxyl O atom. Fig. 1(c–d) showed that the highest occupied molecular orbital (HOMO) and lowest unoccupied molecular orbital (LUMO) is mainly concentrated in the phosphate group and a hydroxyl group, while LUMO mainly falls in the carboxylic group, implying that phosphonic acid group and hydroxyl group are

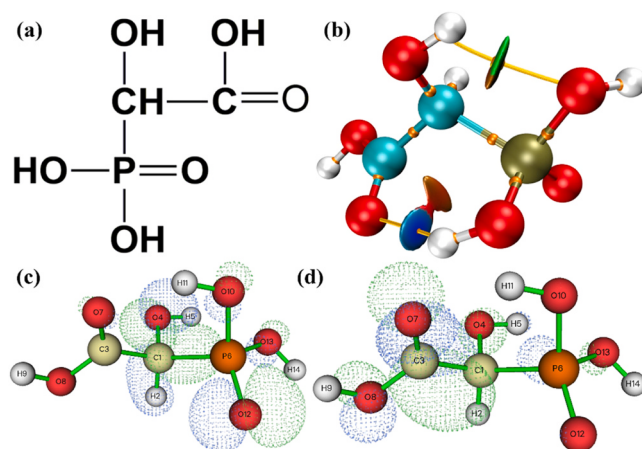
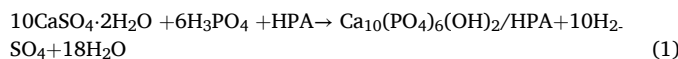


Fig. 1. The structural formula (a) and the optimal configuration of HPA (b) after density functional theory (DFT) calculation (C-cyan, O-red, H-white, P-tan, the dark blue isosurface indicates strong hydrogen bonding between phosphonic acid and carboxyl group, the green slab between phosphonic acid and hydroxyl group refers to the weak H-bond), HOMO (c) and LUMO (d) of HPA molecule.

more likely to provide electrons than the carboxylic group.

2.3. Preparation of HAP used PG as a calcium source

PG waste served as the starting material for the production of nanocrystalline HAP powder. Initially, PG waste was calcined in a Muffle furnace at 600° for 4 h to remove organic impurities, then as a calcium source for preparing HAP, and the main ingredients of PG after calcination were shown in Table S1. The anticipated chemical transformations of preparing HAP took place following the subsequent Eqs. (1–2). The synthesis process for HAP can be summarized as follows [33].



Solution A: 7.692 g PG was blended with water in a 200 mL beaker through robust agitation at ambient conditions for 30 minutes.

Solution B: 0 g, 0.432 g, 0.864 g, 1.296 g, 1.728 g, 2.592 g HPA specimens were combined with 3.459 g, 3.286 g, 3.113 g, 2.94 g, 2.767 g, 2.421 g H₃PO₄ to form phosphorus-containing solutions, respectively. The molar ratio of organophosphate to total phosphorus (organic + inorganic) was 0, 5%, 10%, 15%, 20%, and 30%, correspondingly. With ongoing magnetic stirring and maintaining a temperature of 60 °C, **Solution A** was gradually amalgamated with **Solution B** over a 30-minute interval, while the pH of the mixture was adjusted to approximately 11.0 using an ammonia solution. After 2 hours of stirring, the amalgam was allowed to mature at room temperature for 24 hours. Subsequently, it underwent centrifugation at 4000 r/min and the solid was experienced three cycles of washing with deionized water. Finally, the resultant materials were desiccated in an 80°C oven for 24 hours. The products were then pulverized using a mortar and sifted through a 200-mesh screen. The ultimate samples were designated as HAP, 5HPA-HAP, 10HPA-HAP, 15HPA-HAP, 20HPA-HAP, and 30HPA-HAP. Meanwhile, the remaining solution was evaporated to generate the ammonium sulfate substance.

As described above, in this work, HAP and HPA-HAP composites doped with HAP were prepared by a simple chemical precipitation method, in which waste PG was used as a calcium source, reacted for 2 h in an aqueous solution at 60°, and then aged at room temperature. There is no organic solvent in the whole reaction process, and the reaction temperature is low, which belongs to the low-cost green reaction with

low energy consumption and without organic solvent. Compared with using calcium hydroxide or calcium chloride as a calcium source to prepare HAP, this method has lower raw material cost and solves the problem of secondary pollution and high treatment cost caused by waste PG.

The supplementary materials included explanations of the methods for characterizing, Density Functional Theory (DFT) calculations [51], and Multiwfnd wavefunction analysis [52].

2.4. The batch adsorption and desorption experiments

In different batches of experiments, the influence of the doping amount of HPA, the initial concentration of heavy metal ions, the initial pH of the solution, and contact time on the adsorption performance was explored. In a typical experiment, 25 mg adsorbent was added to a 50 mL solution and stirred continuously for 24 h at 25°C until adsorption reached equilibrium. The separation of solid and liquid was achieved by 0.45 Nylon Filtration, and atomic absorption spectrophotometry (AAS) was used to detect the concentration of residual metal ions infiltrate. All experiments were carried out three times to get an average value, and the error bar in the data graph is the standard deviation (SD). The adsorption capacity (Q_e) of the adsorbents for metal ions and the removal ratio of metal ions were calculated by the following formulas:

$$Q_e = \frac{(C_0 - C_e)V}{m} \quad (3)$$

$$A_e = \frac{C_0 - C_e}{C_0} \times 100\% \quad (4)$$

Where C_0 (mg·L⁻¹) and C_e (mg·L⁻¹) correspond to the initial and residual metal ion concentration, Q_e (mg/g) and A_e are the adsorption capacity of the adsorbent and removal ratio of metal ions (%), respectively. m (g) and V (L) are the mass of the adsorbent and the volume of the solution, respectively.

In the desorption experiments, firstly, 25 mg 20HPA-HAP was first mixed with 50 mL Cd²⁺ (or Co²⁺) solutions (the concentration of heavy metal ions was set as 25 mg/L) and stirred for 24 h. The solid adsorbent was separated by 0.45 Nylon Filtration, then the desorption was carried out by stirring the loaded adsorbent in DI water (or 0.1 M Ca(NO₃)₂) solution for another 24 h. The desorption rate is described as the ratio of the capacity of desorbed Cd²⁺ (or Co²⁺) and adsorbed Cd²⁺ (or Co²⁺).

3. Results and discussion

3.1. Characterizations

In Fig. 2(a-b), the broad absorption band at around 3325 cm⁻¹ in both HAP and 20HPA-HAP was attributed to the OH stretching vibration of HAP. The peaks located at 1092, 1022, 961, 878, 632, 601, and 558 cm⁻¹ were assigned to the characteristic bands of tetrahedral PO₄³⁻ groups of HAP [53]. For HPA, the peaks at 3676, 2972, and 2893 cm⁻¹ were due to the overlapping stretching vibrations of C-H and C-P, and the peak located at 1614 cm⁻¹ corresponded to the stretching vibrations of OH. The peaks at 2364, 2335, 1714, and 1409 cm⁻¹, 1230 cm⁻¹ can be assigned to the carbonyl group (C=O, C-OH) [54–56]. The adsorption at 1087, 1006, 940, and 544 cm⁻¹ could be ascribed to vs (p_O), vs (p=O), and vs (p-OH) [57,58]. In the case of the 20HPA-HAP composite, the peak of 1614 cm⁻¹ blue-shifted to 1589 cm⁻¹, and with the increasing amount of HPA, the intensity of the absorption peak at 1589 cm⁻¹ gradually strengthened. Meanwhile, the peak at 1230 cm⁻¹ red-shifted to 1251 cm⁻¹, while the absorption peaks at 1714 cm⁻¹ and 1087 cm⁻¹ originated from HPA disappeared. Furthermore, the absorption peak at 1022 cm⁻¹ of HAP became a wide absorption band, the peak at 1092 cm⁻¹ disappeared, and the peak intensity at 961 cm⁻¹ and 632 cm⁻¹ decreased with the increase of HPA doping amount. The shift

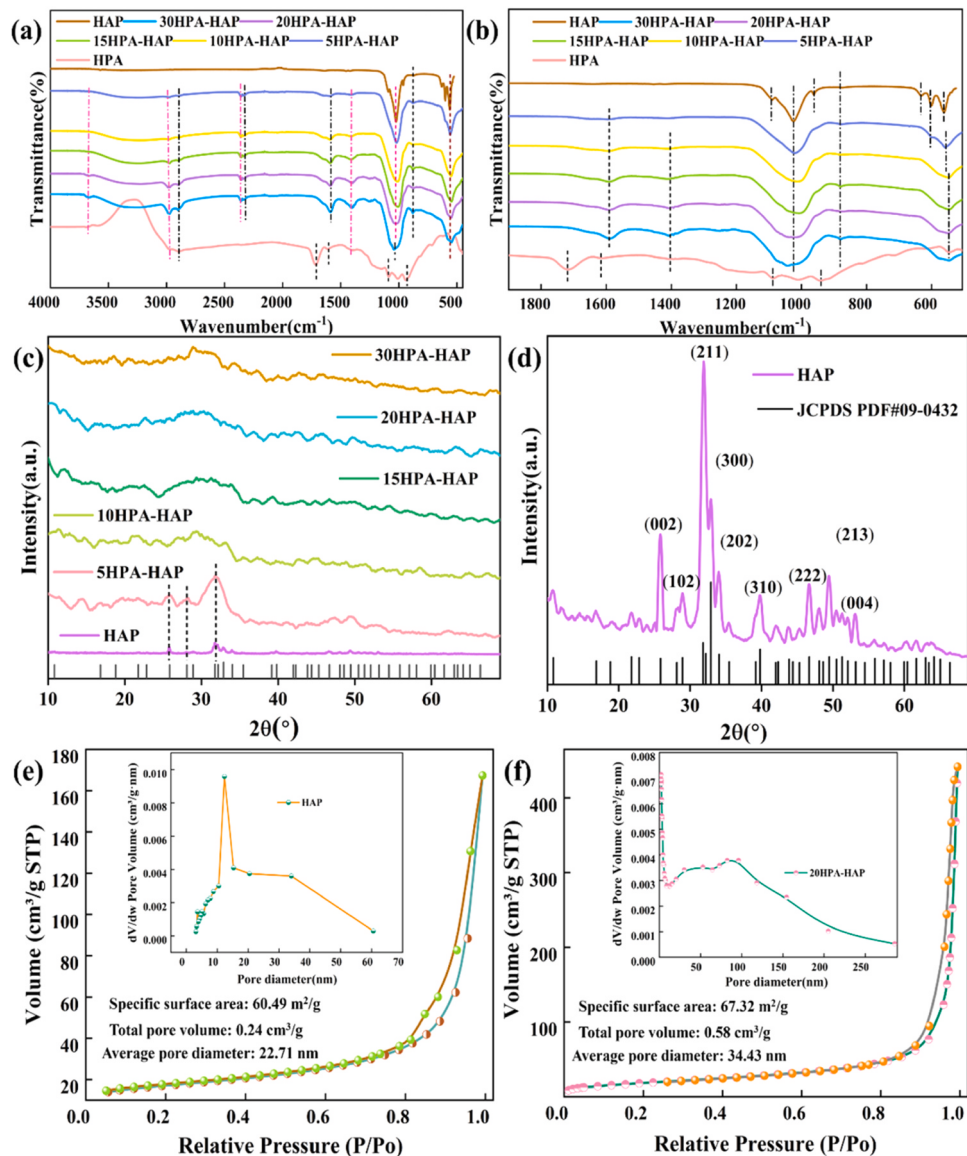


Fig. 2. The characterization of FTIR (a-b), XRD (c-d), BET (e-f).

and intensity of infrared absorption peaks illustrated that HPA and HAP have a strong interaction, the doping of HPA affects the crystallization process of HAP and thus affects the adsorption properties of HAP.

From Fig. 2(c-d), it can be seen that the peaks appeared at $2\theta=25.81^\circ$, 28.92° , 31.89° , 39.78° , 46.69° , 49.45° , and 53.16° corresponded to the (0 0 2), (1 0 2), (2 1 1), (3 1 0), (2 2 2), (2 1 3), and (0 0 4) crystal planes of hydroxyapatite (HAP), respectively, (JCPDS PDF# 09-0432). When HPA was introduced during the synthesis of HAP, the diffraction peak intensities decreased significantly. When the HPA dosage reached 10%, the characteristic diffraction peaks of HAP essentially disappeared, indicating the transformation of HAP into an amorphous state. Therefore, the obtained 10HPA-HAP, 15HPA-HAP, 20HPA-HAP, and 30HPA-HAP all were modified inorganic-organic amorphous calcium phosphate hybrid composite. This confirmed that HPA incorporation had a profound inhibitory effect on HAP crystal growth, which was in good consistent with the FTIR results. The amorphous structure may also be one of the reasons for the improved adsorption performance of HPA-HAP composite for heavy metal ions a phenomenon observed in prior research involving other organic phosphonates [42,59].

In Fig. 2(e-f), the adsorption-desorption isotherms of the two

adsorbents exhibited characteristic type IV behavior with noticeable hysteresis loops, indicating their mesoporous nature. The surface area, total pore volume, and average pore diameter of 20HPA-HAP were $67.32 \text{ m}^2/\text{g}$, $0.58 \text{ cm}^3/\text{g}$, and 34.43 nm , respectively, while that of HAP was $60.49 \text{ m}^2/\text{g}$, $0.24 \text{ cm}^3/\text{g}$ and 22.71 nm , respectively. The specific surface area before and after HPA modification did not change significantly, but the pore volume and pore size of HAP improved, which may also be one of the reasons for the improved adsorption performance of modified HPA-HAP composites for heavy metal pollutants.

In Fig. 3(a-b), HAP displayed a morphology of aggregate short rod-shaped particles with relatively uniform characteristics, whereas the surface of 20HPA-HAP as formed by the aggregation of a large number of irregular micro-spherical particles, making its structure more porous and loosely arranged, with irregular pores that provide more adsorption sites, which was beneficial for the removal of metal ions from wastewater. This was consistent with its XRD characterization and BET characterization results. EDS analysis (Fig. 3(c)) and mapping (Fig. 3(d)) confirmed the presence of carbon (C) in the spectra, signifying the successful incorporation of HPA into HAP.

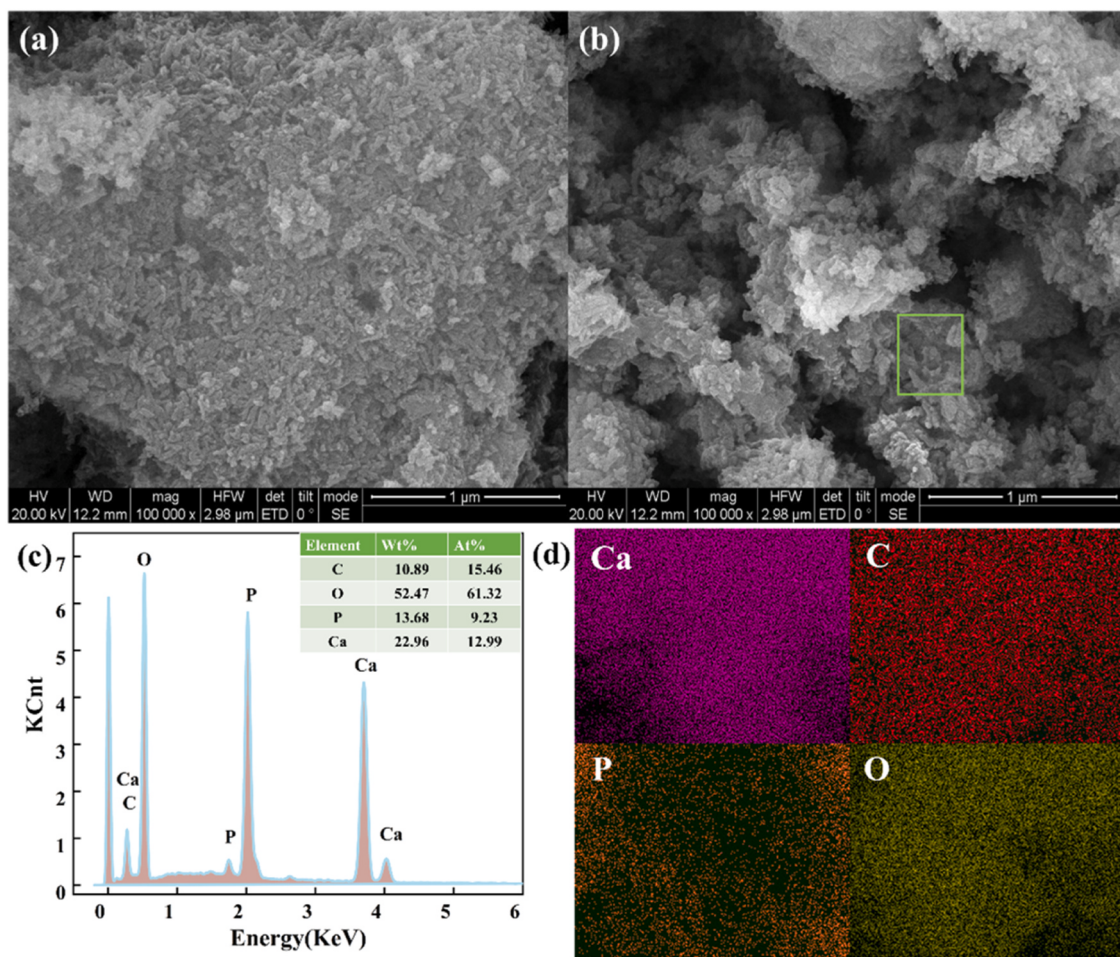


Fig. 3. The SEM (a-HAP, b-20HPA-HAP), EDS (c), and Mapping (d) of 20HPA-HAP.

3.2. Adsorption experiments

3.2.1. Effects of the amount of HPA and the initial concentration of Co^{2+} and Cd^{2+}

Fig. 4(a-b) demonstrated that the addition of HPA significantly amplified HAP's adsorption efficiency and the removal efficiency of Co^{2+} and Cd^{2+} . In the case of synthesized HAP through PG, the adsorption capacity for Co^{2+} and Cd^{2+} stood at 50.12 mg/g and 174.81 mg/g, correspondingly, while the removal efficiency for two heavy metal ions was 12.53% and 21.85%, respectively. When the HPA doping level was elevated from 5% to 20%, the adsorption capacity of 20HPA-HAP for Co^{2+} (with an initial concentration of 200 mg/L) surged from 67.62 mg/g to 111.96 mg/g, and the removal efficiency increased from 16.90% to 27.99%. However, as the HPA quantity continued to rise to 30%, the adsorption performance of the HPA-HAP composite diminished. The phenomenon was similar for the adsorption of Cd^{2+} , when the initial concentration was 400 mg/L, the equilibrium adsorption capacity of 20HPA-HAP reached 418.88 mg/g, with a removal efficiency of 52.36%. Compared to Co^{2+} ions, HAP and 20HPA-HAP adsorbent exhibited better adsorption selectivity for Cd^{2+} ions. The results illustrated that HAP prepared by PG as a calcium source has a good adsorption effect on both heavy metal ions and doping modification of HPA can further improve the adsorption performance of synthesized HAP. In subsequent experiments, undoped HAP and 20HPA-HAP composite were selected as the adsorbent for further probing the adsorption behavior of Co^{2+} and Cd^{2+} .

In Fig. 4(c-d), when pH=8, the adsorption capacity (Q_e) of 20HPA-HAP and HAP for Co^{2+} was 170.96 mg/g and 70.43 mg/g, respectively.

When the concentration of

Cd^{2+} was 400 mg/L, and the Q_e value of the two adsorbents was 460.87 mg/g and 275.84 mg/g, respectively. When the initial concentration (C_0) was set at 50 mg/L, the adsorption capacity of 20HPA-HAP for Co^{2+} and Cd^{2+} measured 62.53 mg/g and 89.17 mg/g, respectively. Q_e exhibited an upward trend with an increase in C_0 . However, the removal efficiency (A_e) of Co^{2+} gradually decreased from 69.54% (with C_0 of 25 mg/L) to 34.08% (with C_0 of 200 mg/L). Within the range of 50–400 mg/L of C_0 , the A_e value of Cd^{2+} exhibited a gradual decline from 89.17% to 57.60%. Remarkably, at equivalent C_0 values for both heavy metal ions, the A_e value of Cd^{2+} greatly exceeded that of Co^{2+} . The adsorption trend of HAP for the two metal ions was similar to this.

3.2.2. Effect of initial solution pH

At 25°C, the pH-dependent distribution of Co^{2+} and Cd^{2+} was computed using Visual MINTEQ software version 3.1 (as depicted in Fig. S1 (a-b)). When higher pH levels induce hydroxide precipitation, it becomes feasible to separate some Co^{2+} and Cd^{2+} through filtration or centrifugation during post-treatment. Nevertheless, accurately quantifying the adsorption capacity for Co^{2+} and Cd^{2+} is challenging in the presence of such precipitation phenomena. To mitigate the impact of precipitation, the adsorption experiments were executed under conditions of $\text{pH} \leq 8.0$, ensuring the solubility of Co^{2+} and Cd^{2+} .

The increased solution pH will affect the further deprotonation of HPA. Fig. S1(c-d) illustrated that all O atoms of deprotonated HPA (for clarity, the positively charged H and P atoms and less negatively charged C atoms were omitted) have a more negative charge than that of the corresponding HPA molecule, so with the increase of pH, it has a

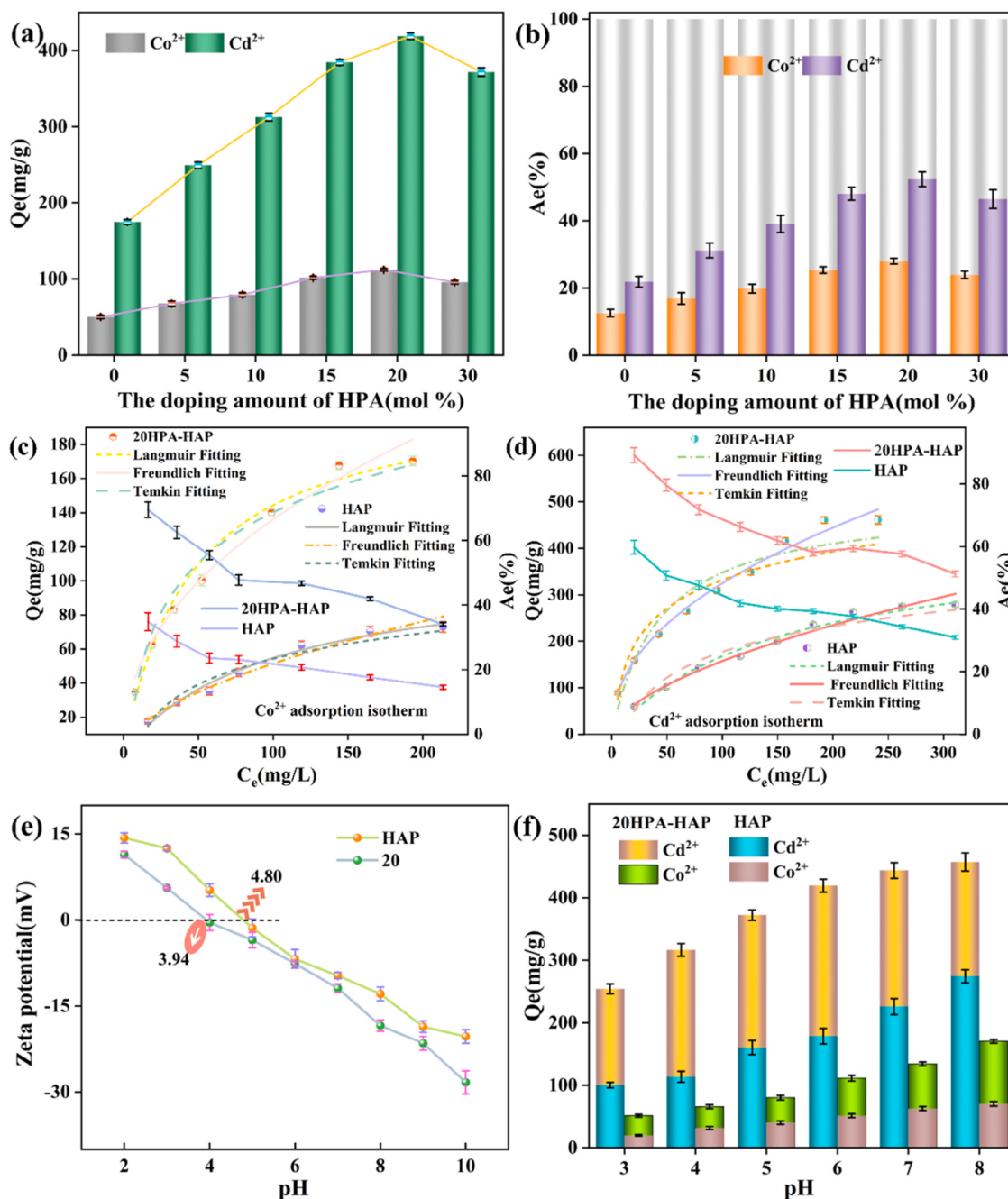


Fig. 4. The effects of the doping amount of HPA (a- Q_e , b- A_e , pH=6.0, $C_0(\text{Co}^{2+}) = 200 \text{ mg/L}$, $C_0(\text{Cd}^{2+}) = 400 \text{ mg/L}$, $t=150 \text{ min}$, $T=25^\circ\text{C}$), the effect of the initial concentration (c- Co^{2+} , d- Cd^{2+} , pH=8.0, $t=150 \text{ min}$, $T=25^\circ\text{C}$), the Zeta potentials of synthesized HAP and 20HPA-HAP (e), the effect of solution pH on the adsorption capacity of HAP and 20HPA-HAP for Co^{2+} and Cd^{2+} (f, $C_0(\text{Co}^{2+}) = 200 \text{ mg/L}$, $C_0(\text{Cd}^{2+}) = 400 \text{ mg/L}$, $t=150 \text{ min}$, $T=25^\circ\text{C}$).

stronger electrophilic effect on positively charged metal ions and thus improves the adsorption effect on heavy metal ions. Meanwhile, the pH of the solution exerts influence over the surface charge of HAP and 20HPA-HAP. As depicted in Fig. 4(e), the pH_{pzc} (pH at the point of zero charge) for HAP and 20HPA-HAP was measured at 4.80 and 3.94, respectively. Consequently, at lower solution pH, the surface charge of the adsorbents becomes positively charged. Furthermore, the electrostatic repulsion led

to a reduction in the adsorption process. Beyond the pH_{pzc} threshold, an escalation in solution pH resulted in heightened negativity of the zeta potential for both HAP and 20HPA-HAP, thereby promoting electrostatic interactions. As illustrated in Fig. 4(f), when the initial solution pH was set at 3.0, the adsorption capacity of 20HPA-HAP for

Cd^{2+} and Co^{2+} was a mere 234.25 mg/g and 50.34 mg/g, respectively. However, as the pH increased, the effectiveness of Co^{2+} and Cd^{2+} separation exhibited a substantial enhancement, when pH=8, the adsorption capacity of 20HPA-HAP for Cd^{2+} and Co^{2+} sharply improved to 468.92 mg/g and 171.38 mg/g. The adsorption of HAP for two heavy metal ions was similar to that of 20HPA-HAP. When pH=8.0, the equilibrium adsorption capacity of HAP for Cd^{2+} and Co^{2+} can reach 275.84 mg/g and 70.63 mg/g.

3.2.3. The adsorption kinetic and adsorption isotherm

The comprehensive details regarding the adsorption dynamics and adsorption isotherms can be found in the [supplementary materials](#), the results were exhibited in Fig. 5(a-b) and Table S2-S5. When considering

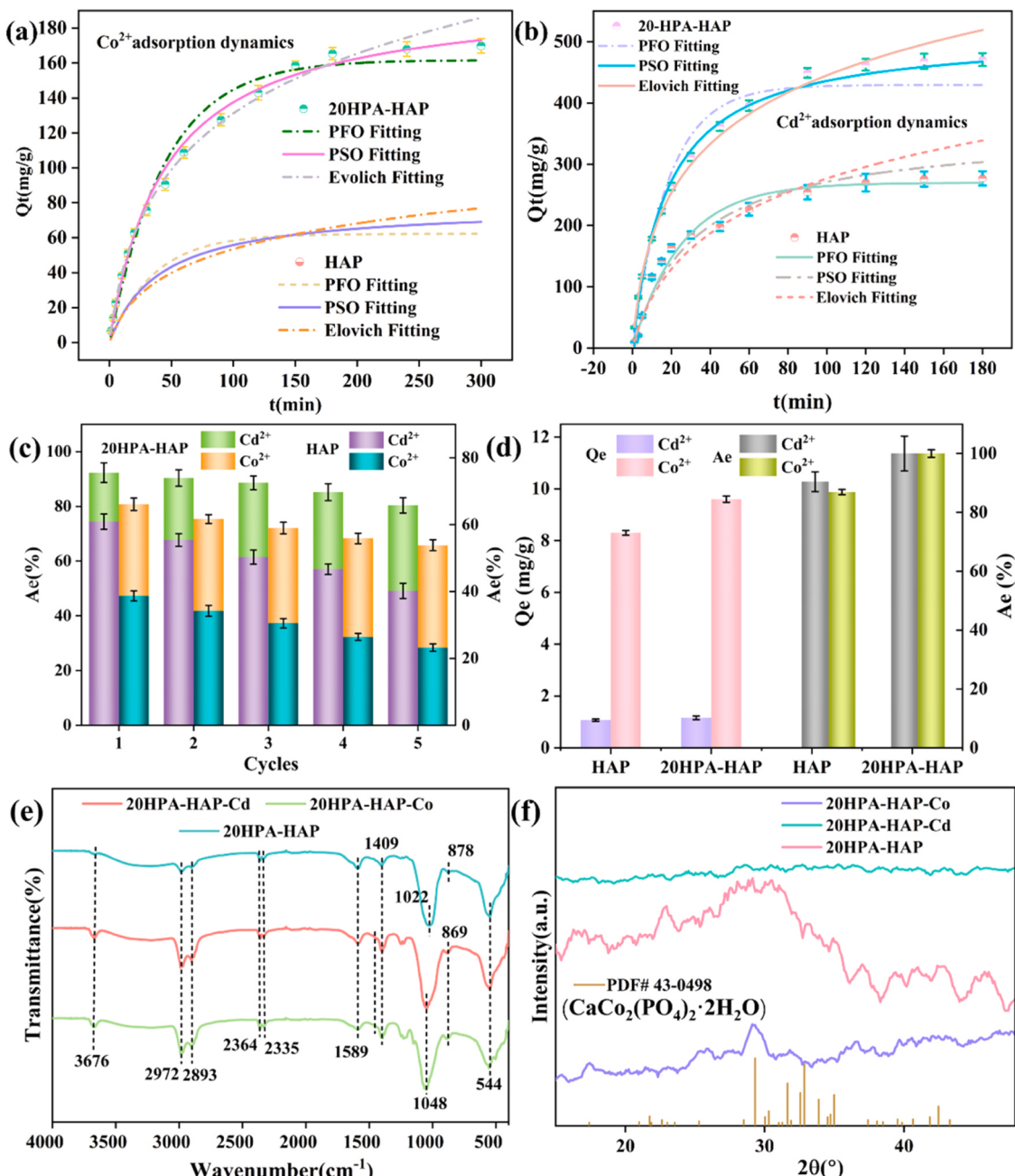


Fig. 5. The adsorption dynamics (a-Co²⁺, b-Cd²⁺), the regeneration of the adsorbents (c, C₀= 25 mg/L, m=20 mg, V=50 mL, t=24 h, T=25°C) and the application in practical wastewater (d , m=10 mg, V=50 mL, t=30 min, T=25°C), the FTIR (e) and XRD (f) characterization of 20HPA-HAP adsorbed Cd²⁺ and Co²⁺.

the adsorption process of Cd²⁺ and Co²⁺ onto 20HPA-HAP, according to the value of R² and χ², it closely adhered to the pseudo-second-order (PSO) and Elovich nonlinear fitting kinetic models. On the other hand, for the adsorption onto HAP, PSO nonlinear fitting kinetic model demonstrated a good fit. As for the isotherm models, the Freundlich model offered a better representation of the adsorption process on 20HPA-HAP and HAP adsorbents for the two heavy metal ions, which indicated that the adsorption process is not simple monolayer adsorption.

3.2.4. The regeneration of the adsorbent and its application in practical wastewater

In Table S6, with the initial concentration of 25 mg/L and pH of 8.0, for the system of HAP-Cd²⁺ and HAP-Co²⁺, in deionized water after 24 h, the adsorption of Cd²⁺ and Co²⁺ was 30.46 mg/g and 19.33 mg/g,

while the desorption capacity was 1.16 mg/g and 0.92 mg/g, so the desorption rate was 3.80% and 4.75%, respectively, implying adsorbed two metal ions on HAP have a certain dissolution. However, the desorption rate of Cd²⁺ and Co²⁺ in 20HPA-HAP-Cd²⁺ and 20HPA-HAP-Co²⁺ was exceedingly low, with values of 0.57% and 0.66%, respectively. This underscores the remarkable immobilization efficacy of 20HPA-HAP on Cd²⁺ and Co²⁺. This feature is of considerable significance because of the irreversible adsorption exhibited by the 20HPA-HAP composite towards Cd²⁺ and Co²⁺. This ensures that once the pollutants are captured, they are firmly retained and do not leach back into aquatic systems throughout the adsorption process [60–62]. This phenomenon can be attributed to the robust chelation of deprotonated HPA with heavy metal ions, forming coordination covalent bonds and creating a ternary complex with HAP (HPA-Metal-HAP).

On the other hand, the regeneration of the adsorbent is highly

significant for its subsequent adsorption of contaminants. Thus, the saturated adsorbent ($C_0 = 25 \text{ mg/L}$, $t = 24 \text{ h}$, $T = 25^\circ\text{C}$, $\text{pH} = 8.0$) was subjected to regeneration using a $0.1 \text{ M Ca}(\text{NO}_3)_2$ solution to assess its recyclability in terms of adsorption performance. As illustrated in

Fig. 5(c), for 20HPA-HAP adsorbent, the removal efficiency for Cd^{2+} decreased from 92.3% to 80.4% after five cycles of adsorption, while the removal efficiency for Co^{2+} decreased from 80.8% to 65.8%. For HAP adsorbent, the value was from 60.9% to 40.2%, from 38.7% to 23.2%, respectively, which suggests that the adsorbents exhibit both reusability and robust regenerative capabilities.

In addition, the adsorption performance of HAP and 20HPA-HAP to Cd^{2+} and Co^{2+} in actual wastewater was explored. The hard-gold electroplating wastewater and cadmium plating wastewater after chemical precipitation, flocculation, and neutralization of an electroplating company contained $0.59 \text{ mg/L Cd}^{2+}$ and 4.8 mg/L Co^{2+} , respectively, which cannot meet the emission standards, the water quality parameters were shown in **Table S7**. Observation (**Fig. 5 (d)**) revealed that the removal efficiency for low-concentration Cd^{2+} and Co^{2+} by 0.2 g/L HAP can reach 90.4% and 86.9%, respectively, and 20HPA-HAP composite can completely remove two types of heavy metal ions from wastewater. This indicated that HAP prepared with PG as a calcium source exhibited excellent removal efficiency for Cd^{2+} and Co^{2+} in actual wastewater, and the adsorption properties of HPA/HAP composites modified by HPA doping were further improved. In addition, keeping other conditions unchanged, we also used calcium nitrate instead of PG as calcium source to prepare HAP. Under the same optimal experimental conditions, it was found that its equilibrium adsorption

capacity for Cd^{2+} and Co^{2+} was 281.02 mg/g and 74.48 mg/g , respectively, which indicated that PG could be used as a raw material for preparing HAP. **Table 1** showed the comparison of adsorption capacity (Q_e) for Cd^{2+} and Co^{2+} with various adsorbents.

3.3. The adsorption mechanisms of HPA-incorporated HAP composite

3.3.1. The characterizations after adsorption of two metal ions

In **Fig. 5(e)**, the FTIR analysis post- Co^{2+} and Cd^{2+} adsorption onto the 20HPA-HAP composite was depicted. After adsorption, 20HPA-HAP- M^{2+} ($\text{M}=\text{Co}, \text{Cd}$) exhibited the emergence of a new absorption peak at 1455 cm^{-1} , meanwhile, the absorption peaks at $1251, 1022$, and 878 cm^{-1} shifted to $1240, 1048$, and 869 cm^{-1} , respectively. These alterations in FTIR spectra signified the occurrence of coordination reactions during the adsorption of Co^{2+} and Cd^{2+} by 20HPA-HAP, with the new peaks attributed to the complexation of Co^{2+} and Cd^{2+} with the surface functional groups of 20HPA-HAP [90]. **Fig. 5(f)** revealed that after the adsorption of the 20HPA-HAP composite for Co^{2+} , distinct diffraction peaks indicative of $\text{CaCo}_2(\text{PO}_4)_2 \cdot 2 \text{ H}_2\text{O}$ emerged. This implied that the Co^{2+} adsorption mechanism by 20HPA-HAP involved dissolution-precipitation processes. Conversely, post- Cd^{2+} adsorption, the XRD pattern adopted an amorphous nature resembling that of 20HPA-HAP, without evident formation of additional crystalline phases, the dominant adsorption mechanism of 20HPA-HAP for Cd^{2+} involved surface complexation. In addition, **Fig. S2** was the full spectrum of XPS before and after adsorption of heavy metal ions by the adsorbent 20HPA-HAP, from which it can be seen that XPS contained Ca, C, P, and O elements before adsorption, and new characteristic peaks of Cd or Co appeared after adsorption, indicating the effective capture of the two heavy metal ions by 20HPA-HAP.

Except for the above characterization, the concentration of Ca^{2+} , total phosphate, and organophosphorus in solution after adsorption was detected. The result exhibited in **Table S10**, it can be seen that after adsorption, the solution contains 31.9 and $34.4 \text{ mg/L Ca}^{2+}$, respectively, indicating that the adsorption of the two metal ions by 20HPA-HAP composite involved an ion exchange mechanism [91]. The content of total phosphorus and organophosphorus in solution after adsorption was very low, which indicated that the adsorbent has good stability.

Table 1
Comparison of adsorption capacity of Cd^{2+} and Co^{2+} on various adsorbents.

Adsorbents	The adsorption capacity (mg/g)	Reference
FGD-HAP	43.10 (Cd^{2+})	[63]
Biopolymer-coated HAP	35.52 (Cd^{2+})	[64]
Bamboo charcoal	12.08 (Cd^{2+})	[65]
AC-T	25.1 (Cd^{2+})	[66]
3D-SRGO	234.8 (Cd^{2+})	[67]
Granular activated carbon oxide	30.8 (Cd^{2+})	[68]
Indonesian peat	14.0 (Cd^{2+})	[69]
Iminodiacetate chelating resins	111.3 (Cd^{2+})	[70]
Magnetic chelating resin	224.8 (Cd^{2+})	[71]
ZnAl-LDH	93.3 (Cd^{2+})	[72]
IDA-chelating resins	68.6 (Cd^{2+})	[73]
NZP	214.7 (Cd^{2+})	[74]
GSCB	222 (Cd^{2+})	[75]
phosphate-embedded calcium alginate beads	82.64 (Co^{2+})	[76]
EDTAD modified orange peel	51.02 (Cd^{2+}), 40.49 (Co^{2+})	[77]
Amination graphene oxide	116.3 (Co^{2+})	[78]
$\text{Fe}_3\text{O}_4/\text{Bentonite}$	18.7 (Co^{2+})	[79]
Macroporous strong acid resin	21.9 (Co^{2+})	[80]
Dowex 50 W-x8 resin	52.6 (Co^{2+})	[81]
Nano-NaX zeolite	125.3 (Co^{2+})	[82]
Chitosan-montmorillonite	150 (Co^{2+})	[83]
HAP	22.53 (Co^{2+})	[84]
Hydroxyapatite Beads	11.35 (Co^{2+})	[85]
hydroxyapatite/ $\text{Fe}_3\text{O}_4/\text{polydopamine}$ magnetic nanocomposite	49.32 (Co^{2+})	[86]
	322.6 (Cd^{2+}), 294.1 (Co^{2+})	[87]
$\text{Fe}_3\text{O}_4@\text{TAS}$	370 (Cd^{2+}), 270 (Co^{2+})	[88]
ATMP-doping HAP	321.26 (Cd^{2+})	[44]
HD- MHAP ^a	172.3 (Co^{2+})	[89]
Alendronate-doping HAP	469(Cd^{2+})	[59]
HAP (PG as calcium source)	275.84 (Cd^{2+}), 70.63 (Co^{2+})	This work
HAP ($\text{Ca}(\text{NO}_3)_2$ as calcium source)	281.02 (Cd^{2+}), 74.48 (Co^{2+})	
20HPA-HAP	468.92 (Cd^{2+}), 171.38 (Co^{2+})	

^a : Magnetic Hexamethylene diamine tetramethylene phosphonic acid (HDTMP)-hydroxyapatite

3.3.2. Visual interaction between HPA and two heavy metal ions

In **Fig. S1(d)**, the atomic charge analysis of O atoms within the PO_3^{2-} moiety of H_2L^{2-} revealed a significantly pronounced negative charge. This observation implied a heightened propensity for electrophilic interactions between Cd^{2+} or Co^{2+} and the O atoms in the PO_3^{2-} group. In AIM (Atoms in Molecules) theory, in instances of similar chemical bonds, increased electron density ($\rho(\text{BCP})$) and a more negative potential energy density ($V(\text{BCP})$) at the bond critical point (BCP) signify a stronger chemical bond. It is crucial to highlight that an energy density ($H(\text{BCP}) < 0$) is a prerequisite for a covalent bond [92], and a more negative Bond Degree ($\text{BD} = H(\text{BCP})/\rho(\text{BCP})$) indicates a greater affinity [93]. **Fig. 6(a-b)** demonstrated that the BCPs of O-Cd and O-Co bonds exhibited characteristics typical of covalent bonds: $\rho(\text{BCP}) > 0$, $V(\text{BCP}) < 0$, $H(\text{BCP}) < 0$, elucidating the formation of O-Cd or O-Co covalent bonds [43]. Additionally, in comparison to O-Co, it was evident that the O-Cd bond possesses higher $\rho(\text{BCP})$, more negative $V(\text{BCP})$, and BD values. This observation indicated that the bond strength of the O-Cd bonds was superior to that of the O-Co bonds. This distinction could contribute to the enhanced adsorption capacity of HPA-modified HAP for Cd ions compared to cobalt ions.

The examination of the Electron Localization Function (ELF) in **Fig. 6(c-d)** illustrated an electron concentration surrounding the O atoms of the PO_3^{2-} group in H_2L^{2-} . This additional observation supports the covalent character of both O-Cd and O-Co bonds, with O-Cd bonds exhibiting greater strength compared to O-Co bonds.

Analysis of Bond Order Density (BOD) [94] (**Fig. 6(e-f)**) and Natural Adaptive Orbital (NAO) [95] in **Fig. 7** depicted the interaction between

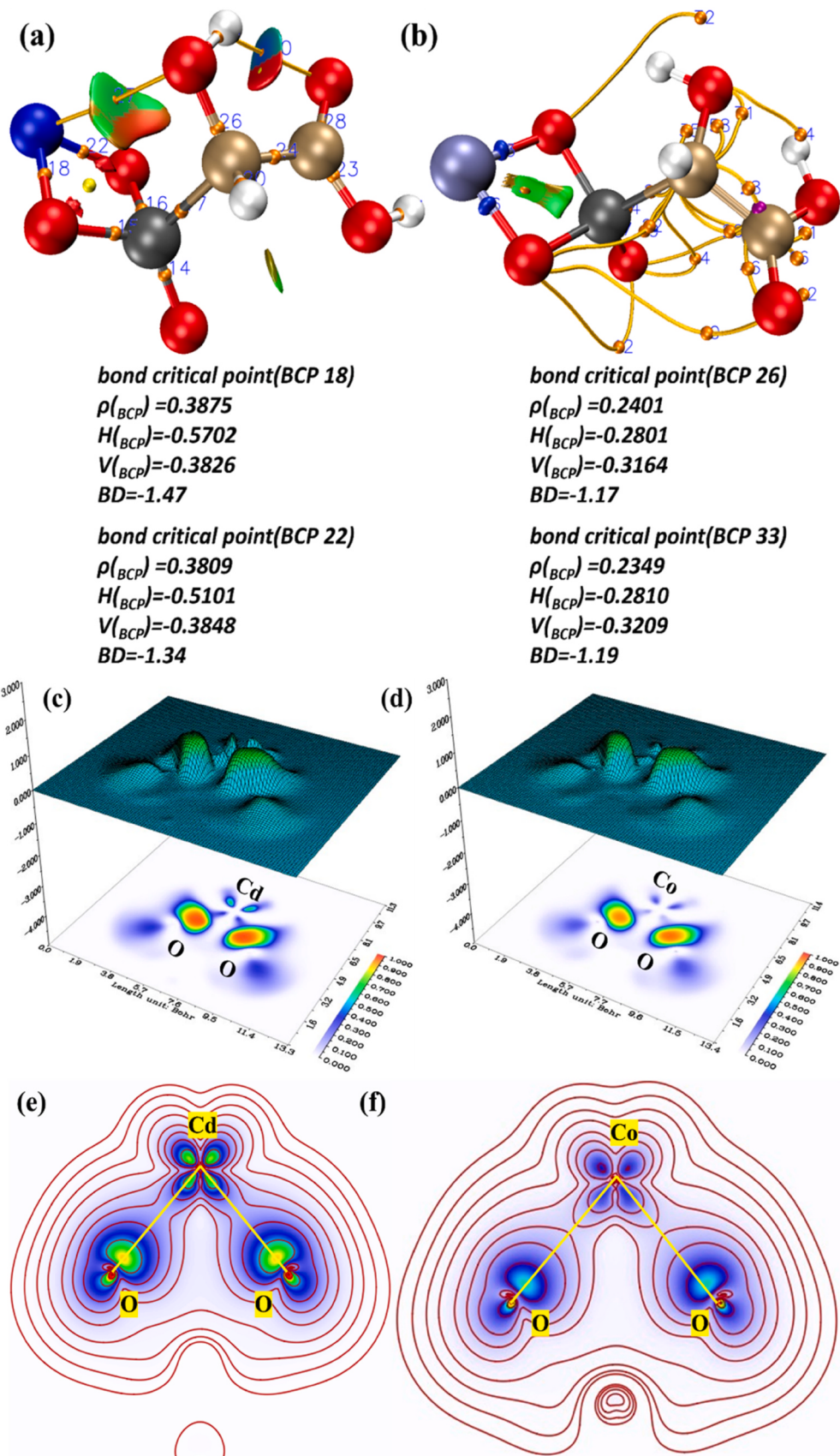


Fig. 6. The AIM topology analysis of HPA-Cd (a) and HPA-Co (b); the shaded surface map with projection effect of ELF of $\text{H}_2\text{L}^{2-}\text{-Cd}$ (c) and $\text{H}_2\text{L}^{2-}\text{-Co}$ (d), the color-filled map of BOD isosurface of $\text{H}_2\text{L}^{2-}\text{-Cd}$ (e) and $\text{H}_2\text{L}^{2-}\text{-Co}$ (f) (C-tan, H-white, O-red, P-gray, Cd-blue, Co-ice-blue).

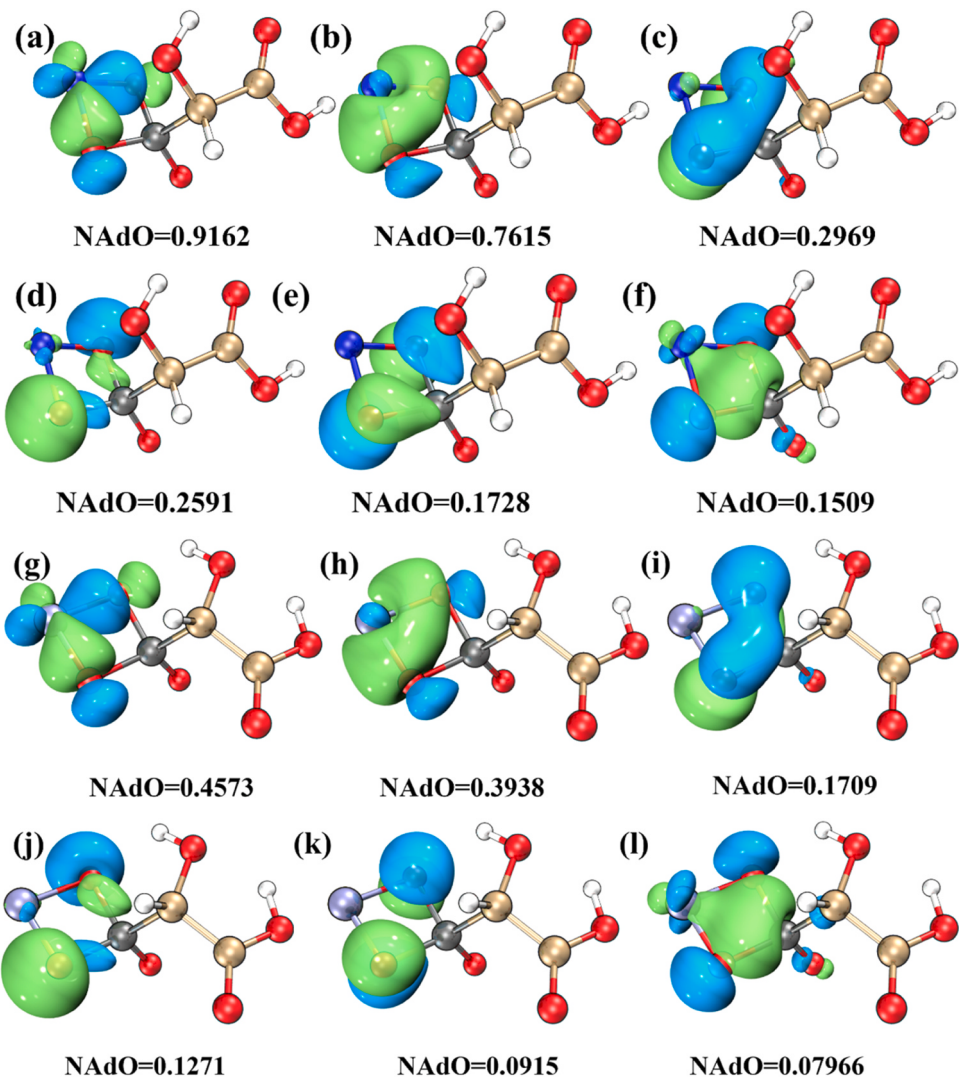


Fig. 7. The main NAdO of H₂L²⁻-Cd (a-f) and H₂L²⁻-Co (g-l).

O atoms of deprotonated HPA with Cd²⁺ or Co²⁺ ions. Additionally, it is noticeable that the BOD strength of the O-Cd bonds was markedly superior to that of the O-Co bond (the electron density of O atoms in O-Cd bonds was distinctly higher than that of O-Co bonds; the redder color indicates greater electron density), which may be one of the reasons that the HPA-HAP composite adsorbent has better adsorption performance for Cd²⁺. This observation aligned with the findings from AIM and ELF analyses.

In addition, the analysis provided in Table S8 from the NAdO indicated significant contributions of two NAdO orbitals to the bonding orbital of O-Cd or O-Co. For O-Cd, the highest NAdO eigenvalue recorded was 0.9162 (NAdO 1), corresponding to the involvement of O₁₀, O₁₁, and Cd₁₃ at percentages of 33.61%, 34.64%, and 31.10%, respectively. This finding further corroborated that oxygen atoms contribute lone pair electrons to chelate with Cd, forming coordination covalent bonds. The analysis of O-Co NAdO orbitals was similar to this analysis. HPA and HAP have strong interaction, and the phosphonic acid group oxygen atom of HPA formed a covalent coordination bond with metal ions and then formed a stable HAP-M²⁺-HPA surface complex, which greatly improved the adsorption performance for metal ions.

4. Conclusions

The study successfully develops a novel and efficient method for the

adsorption of heavy metal ions using amorphous calcium phosphate derived from phosphogypsum as a calcium source and HPA as a dopant. The main conclusions are as follows:

- (1) With PG as a calcium source, the adsorption capacity of the HPA-HAP composite for cadmium and cobalt ions can be greatly improved by doping HAP modification with HPA. The adsorption capacity of the modified composite for cadmium and cobalt was 1.7 times and 2.4 times that of HAP, respectively.
- (2) PSO and Elovich nonlinear fitting kinetic models were more suitable for describing the adsorption process of 20HAP-HAP for two metals. Meanwhile Freundlich model offered a better representation of the adsorption process, which indicated that the adsorption process is not simple monolayer adsorption.
- (3) For actual wastewater, it revealed that the removal efficiency for low-concentration Cd²⁺ and Co²⁺ by 0.2 g/L HAP can reach 90.4% and 86.9%, respectively, and 20HAP-HAP composite can completely remove two types of heavy metal ions from wastewater. HPA-HAP composite using waste PG as a calcium source is expected to be applied to practical wastewater treatment due to the green preparation process and low cost. Meanwhile, the realization of the comprehensive utilization of PG waste in the present work, not only offers a viable solution for mitigating

- heavy metal pollution but also exemplifies a sustainable approach by repurposing industrial waste.
- (4) The dominant adsorption mechanism of 20HPA-HAP for Cd²⁺ involved surface complexation. For the adsorption of Co²⁺ onto 20HPA-HAP composite, the adsorption mechanism involved surface complexation and dissolution-precipitation processes. The strength of the O-Cd bonds was significantly stronger than that of the O-Co bonds, which contributed to the enhanced adsorption capacity of HPA-modified HAP for Cd ions compared to cobalt ions.

CRediT authorship contribution statement

Zhongtian Dong: Software, Formal analysis, Data curation. **Zhiren Zhao:** Writing – original draft, Methodology, Data curation. **Mingzhu Xia:** Writing – review & editing, Supervision, Resources, Project administration. **Fengyun Wang:** Writing – review & editing, Supervision, Resources, Funding acquisition. **Fenghe Wang:** Writing – review & editing, Project administration, Conceptualization.

Declaration of Competing Interest

The authors declare that they have no known competing financial interests or personal relationships that could have appeared to influence the work reported in this paper.

Data Availability

No data was used for the research described in the article.

Acknowledgments

The authors would like to acknowledge the financial support of the National Natural Science Foundation of China (52072180). The work was also supported by The Urgently Needed Talent Introduction Projects of Key Support Areas of Shandong Province (2204-370402-04-01-853416).

Appendix A. Supporting information

Supplementary data associated with this article can be found in the online version at [doi:10.1016/j.jece.2024.112994](https://doi.org/10.1016/j.jece.2024.112994).

References

- [1] I.F. Nata, C.K. Lee, Novel carbonaceous nanocomposite pellicle based on bacterial cellulose, <https://doi.org/10.1016/j.GreenChem.2010.07.020>, <https://doi.org/10.1039/c003479g>.
- [2] J.C. Callura, K.M. Perkins, C.W. Noack, N.R. Washburn, D.A. Dzombak, A. K. Karamalidis, Selective adsorption of rare earth elements onto functionalized silica particles, <https://doi.org/10.1016/j.GreenChem.2018.01.020>, <https://doi.org/10.1039/c8gc00051d>.
- [3] X. Wang, R. Zhang, Z. Li, B. Yan, Adsorption properties and influencing factors of Cu(II) on polystyrene and polyethylene terephthalate microplastics in seawater, <https://doi.org/10.1016/j.Scitotenv.2022.152573>, <https://doi.org/10.1016/j.Scitotenv.2022.152573>.
- [4] M. Abbasi, E. Safari, M. Baghdadi, M. Janmohammadi, Enhanced adsorption of heavy metals in groundwater using sand columns enriched with graphene oxide: lab-scale experiments and process modeling, <https://doi.org/10.1016/j.j.WaterProcessEng.2021.101961>.
- [5] M. Bilal, I. Ihsanullah, What makes MXenes emergent materials for the adsorption of heavy metals from water? A critical review, <https://doi.org/10.1016/j.j.WaterProcessEng.2022.103010>.
- [6] R. Duan, C.B. Fedler, X. Li, X. Jiao, Co-transport of Cu²⁺, Pb²⁺, Cd²⁺, and Zn²⁺ in the columns of polyaluminum chloride and anionic polyacrylamide water treatment residuals, <https://doi.org/10.1016/j.j.WaterProcessEng.2022.102475>.
- [7] Y. Guo, Y. Huang, J. Li, S. Ouyang, B. Fan, Y. Liu, Study on dynamic adsorption characteristics of gangue to heavy metals in goaf and its water purification mechanism under leaching condition, <https://doi.org/10.1016/j.j.WaterProcessEng.2023.103741>.
- [8] X. Huang, L. Lang, J. Li, C.S. Poon, Synthesis of Na-A zeolite loaded bentonite and its application for removal of Cu(II) from aqueous solutions, <https://doi.org/10.1016/j.j.WaterProcessEng.2023.104359>.
- [9] N. Kitikova, A. Ivanets, I. Shashkova, L. Kul'bitskaya, O. Baigenzhenov, M. Sillanpaa, Sorption of Pb²⁺ and Zn²⁺ ions on Zr-Ca-Mg phosphates: kinetics and mechanism studies, <https://doi.org/10.1016/j.j.WaterProcessEng.2023.103725>.
- [10] K. Pyrzynska, Removal of cadmium from wastewaters with low-cost adsorbents, <https://doi.org/10.1016/j.j.EnvChemEng.2019.102795>.
- [11] J.O. Eniola, B. Sizirici, Y. Fseha, J.F. Shaheen, A.M. Abouella, Application of conventional and emerging low-cost adsorbents as sustainable materials for removal of contaminants from water, <https://doi.org/10.1016/j.j.EnvSciPollutRes.2023.88245-88271>.
- [12] A. Saraeian, A. Hadi, F. Raji, A. Ghassemi, M. Johnson, Cadmium removal from aqueous solution by low-cost native and surface modified Sorghum x drummondii (Sudangrass), <https://doi.org/10.1016/j.j.EnvChemEng.2018.05.018>.
- [13] H.-J. Hong, J. Kim, I.-H. Yoon, G. Yoo, E.J. Kim, J. Ahn, J.-W. Yang, Preparation of Low-Cost Adsorbents from Paper Industry Wastes and their Pb(II) Removal Behavior in Water, <https://doi.org/10.1016/j.j.SepSciTech.2014.2540-2547>.
- [14] E.P. Puglla, D. Guaya, C. Tituana, F. Osorio, M.J. García-Ruiz, Biochar from Agricultural by-Products for the Removal of Lead and Cadmium from Drinking Water, <https://doi.org/10.1016/j.j.Water.2020.13390/w12102933>.
- [15] G. He, C. Wang, J. Cao, L. Fan, S. Zhao, Y. Chai, Carboxymethyl chitosan-kaolinite composite hydrogel for efficient copper ions trapping, <https://doi.org/10.1016/j.j.EnvChemEng.2019.102953>.
- [16] Y. Zheng, J. Zhang, Experimental study on the adsorption of dissolved heavy metals by nano-hydroxyapatite, <https://doi.org/10.1016/j.j.WaterSciTechnol.2020.1825-1832>.
- [17] M. Prakash, T. Lemaire, D. Di Tommaso, N. de Leeuw, M. Lewerenz, M. Caruel, S. Naili, Transport properties of water molecules confined between hydroxyapatite surfaces: A molecular dynamics simulation approach, <https://doi.org/10.1016/j.j.apusc.2017.02.029>.
- [18] N. Jing, A.N. Zhou, Q.H. Xu, The synthesis of super-small nano hydroxyapatite and its high adsorptions to mixed heavy metallic ions, <https://doi.org/10.1016/j.j.HazardMater.2018.02.049>.
- [19] H. Wu, D. Xu, M. Yang, X. Zhang, Surface structure of hydroxyapatite from simulated annealing molecular dynamics simulations, <https://doi.org/10.1016/j.j.Langmuir.2016.06.046>.
- [20] W. Zhao, Z. Xu, Y. Yang, N. Sahai, Surface energetics of the hydroxyapatite nanocrystal-water interface: a molecular dynamics study, <https://doi.org/10.1016/j.j.Langmuir.2014.07.058>.
- [21] T.-J. Lin, Predicting binding affinities of nitrogen-containing bisphosphonates on hydroxyapatite surface by molecular dynamics, <https://doi.org/10.1016/j.j.ChemPhysLett.2019.08.008>.
- [22] M.H. Su, Z.Q. Liu, Y.H. Wu, H.R. Peng, T. Ou, S. Huang, G. Song, L.J. Kong, N. Chen, D.Y. Chen, Graphene oxide functionalized with nano hydroxyapatite for the efficient removal of U(VI) from aqueous solution, <https://doi.org/10.1016/j.j.EnvPol.2021.268>.
- [23] M. Su, D.C.W. Tsang, X. Ren, Q. Shi, J. Tang, H. Zhang, L. Kong, L. Hou, G. Song, D. Chen, Removal of U(VI) from nuclear mining effluent by porous hydroxyapatite: Evaluation on characteristics, mechanisms and performance, <https://doi.org/10.1016/j.j.EnvPol.2019.07.059>.
- [24] Y. Liu, R. Zhang, Z. Sun, Q. Shen, Y. Li, Y. Wang, S. Xia, J. Zhao, X. Wang, Remediation of artificially contaminated soil and groundwater with copper using hydroxyapatite/calcium silicate hydrate recovered from phosphorus-rich wastewater, <https://doi.org/10.1016/j.j.EnvPol.2021.115978>.
- [25] Y.-Y. Wang, Y.-X. Liu, H.-H. Lu, R.-Q. Yang, S.-M. Yang, Competitive adsorption of Pb(II), Cu(II), and Zn(II) ions onto hydroxyapatite-biochar nanocomposite in aqueous solutions, <https://doi.org/10.1016/j.j.SolidStateChem.2018.02.010>.
- [26] H. Guo, C. Jiang, Z. Xu, P. Luo, Z. Fu, J. Zhang, Synthesis of bitter gourd-shaped nanoscaled hydroxyapatite and its adsorption property for heavy metal ions, <https://doi.org/10.1016/j.j.MaterLett.2019.01.028>.
- [27] Q.U. Ain, H. Zhang, M. Yaseen, U. Rasheed, K. Liu, S. Subhan, Z. Tong, Facile fabrication of hydroxyapatite-magnetite-bentonite composite for efficient adsorption of Pb(II), Cd(II), and crystal violet from aqueous solution, <https://doi.org/10.1016/j.j.CleanProd.2020.119088>.
- [28] A. Haider, S. Haider, S.S. Han, I.-K. Kang, Recent advances in the synthesis, functionalization and biomedical applications of hydroxyapatite: a review, <https://doi.org/10.1016/j.j.RSCAdv.2017.7442-7458>.

- [29] M. Ibrahim, M. Labaki, J.-M. Giraudon, J.-F. Lamonier, Hydroxyapatite, a multifunctional material for air, water and soil pollution control: A review, <https://doi.org/10.1016/j.hazmat.2019.121139>.
- [30] A. Fihri, C. Len, R.S. Varma, A. Solhy, Hydroxyapatite: a review of syntheses, structure and applications in heterogeneous catalysis, <https://doi.org/10.1016/j.coord.2017.06.009>.
- [31] M. Prakasam, J. Locs, K. Salma-Ancane, D. Loca, A. Largeau, L. Berzina-Cimdina, Fabrication, properties and applications of dense hydroxyapatite: a review, <https://doi.org/10.1016/j.jfunctbiomater.2015.1099-1140>.
- [32] N. Aslan, G. Özçayan, Adsorptive removal of lead-210 using hydroxyapatite nanopowders prepared from phosphogypsum waste, <https://doi.org/10.1016/j.jradioanalnuclchem.2019.1023-1028>.
- [33] S. Mousa, A. Hanna, Synthesis of nano-crystalline hydroxyapatite and ammonium sulfate from phosphogypsum waste, <https://doi.org/10.1016/j.materresbull.2012.11.067>.
- [34] S.M. Mousa, N.S. Ammar, H.A. Ibrahim, Removal of lead ions using hydroxyapatite nano-material prepared from phosphogypsum waste, <https://doi.org/10.1016/j.jscs.2014.12.006>.
- [35] B. Bouargane, K. Laaboubi, M.G. Biyoune, B. Bakiz, A. Atbir, Effective and innovative procedures to use phosphogypsum waste in different application domains: review of the environmental, economic challenges and life cycle assessment, <https://doi.org/10.1016/j.jmatercycleswaste.2023.1288-1308>.
- [36] D. Zhang, H. Luo, L. Zheng, K. Wang, H. Li, Y. Wang, H. Feng, Utilization of waste phosphogypsum to prepare hydroxyapatite nanoparticles and its application towards removal of fluoride from aqueous solution, <https://doi.org/10.1016/j.jhazmat.2012.09.066>.
- [37] S.M. Mousa, N.S. Ammar, H.A. Ibrahim, Removal of lead ions using hydroxyapatite nano-material prepared from phosphogypsum waste, <https://doi.org/10.1016/j.jscs.2014.12.006>.
- [38] H. Bensalah, S.A. Younssi, M. Ouammou, A. Gurlo, M.F. Bekheet, Azo dye adsorption on an industrial waste-transformed hydroxyapatite adsorbent: Kinetics, isotherms, mechanism and regeneration studies, <https://doi.org/10.1016/j.jece.2020.103807>.
- [39] H. Bensalah, M.F. Bekheet, S. Alami Younssi, M. Ouammou, A. Gurlo, Hydrothermal synthesis of nanocrystalline hydroxyapatite from phosphogypsum waste, <https://doi.org/10.1016/j.jenvironchem.2018.01.052>.
- [40] S. Saeiabi, A. Gouza, H. Bouyarmane, A. Laghzizil, A. Saeiabi, Organophosphonate-modified hydroxyapatites for Zn(II) and Pb(II) adsorption in relation of their structure and surface properties, <https://doi.org/10.1016/j.jenvironchem.2016.11.036>.
- [41] Y. Daniels, N. Lyczko, A. Nizhoi, S.D. Alexandratos, Modification of Hydroxyapatite with Ion-Selective Complexants: 1-Hydroxyethane-1,1-diphosphonic Acid, <https://doi.org/10.1021/je504181z>.
- [42] X. Fang, S. Zhu, J. Ma, F. Wang, H. Xu, M. Xia, The facile synthesis of zoledronate functionalized hydroxyapatite amorphous hybrid nanobiomaterial and its excellent removal performance on Pb²⁺ and Cu²⁺, <https://doi.org/10.1016/j.jhazmat.2020.122291>.
- [43] Z. Zhao, X. Zhang, D. Ruan, H. Xu, F. Wang, W. Lei, M. Xia, Efficient removal of heavy metal ions by diethylenetriaminepenta(methylene phosphonic) acid-doped hydroxyapatite, <https://doi.org/10.1016/j.scitotenv.2022.157557>.
- [44] Y. Zhang, M. Xia, F. Wang, J. Ma, Experimental and theoretical study on the adsorption mechanism of Amino trimethylphosphate (ATMP) functionalized hydroxyapatite on Pb (II) and Cd (II), <https://doi.org/10.1016/j.colsurfa.2021.127029>.
- [45] J. Liu, L. Hu, Y. Liu, T. Zhu, Z. Wang, G. Pan, The effect of 2-hydroxyphosphonoacetic acid on the removal rate selectivity of Cu/Co/TEOS in H₂O₂ based alkaline slurries, <https://doi.org/10.1016/j.ecss.2021.114001>.
- [46] T. Zhai, R. Yan, W. He, H. Ma, Corrosion protection performance of Mo-incorporated 2-hydroxyphosphonoacetic acid-Zn²⁺-complex conversion layers on the cold-rolled steel substrate, <https://doi.org/10.1016/j.surfcoat.2018.07.049>.
- [47] Y. Gao, L. Ward, L. Fan, H. Li, Z. Liu, A study of the use of polyaspartic acid derivative composite for the corrosion inhibition of carbon steel in a seawater environment, <https://doi.org/10.1016/j.jmolliq.2019.111634>.
- [48] H. Lin, Y. Wang, An organic phosphonic acid doped polyaniline/zirconia/epoxy composite coating for metal protection in the marine environment, <https://doi.org/10.1016/j.progorgcoat.2023.107671>.
- [49] D.-P. Dong, J. Li, Z.-G. Sun, X.-F. Zheng, H. Chen, L. Meng, Y.-Y. Zhu, Y. Zhao, J. Zhang, Hydrothermal synthesis, crystal structure, and thermal stability of a novel 3D cadmium phosphonate with double-stranded helical channels, <https://doi.org/10.1016/j.inorgchemcomm.2007.06.008>.
- [50] M. yang, Y. Zhou, D. Zhang, F. Zhou, H. Ning, M. He, R. Chi, W. Yin, Highly effective and selective recovery of Gd(III) from wastewater by defective MOFs-based ion-imprinted polymer: Performance and mechanism, <https://doi.org/10.1016/j.cej.2023.145782>.
- [51] M.J. Frisch, gaussian09, (<http://www.gaussian.com/>) (2009).
- [52] T. Lu, F. Chen, Quantitative analysis of molecular surface based on improved Marching Tetrahedra algorithm, <https://doi.org/10.1016/j.jmgm.2012.07.004>.
- [53] C. Garbo, M. Sindilaru, A. Carlea, G. Tomoia, V. Almasan, I. Petean, A. Mocanu, O. Horovitz, M. Tomoia-Cotisel, Synthesis and structural characterization of novel porous zinc substituted nanohydroxyapatite powders, <https://doi.org/10.1016/j.partsci.2017.29-37>.
- [54] C.J. Zou, Q.W. Tang, G.H. Lan, Q. Tian, T.Y. Wang, Enhancement inhibition efficiency of PBTCA depending on the inclusion complex with hydroxypropyl- β -cyclodextrin, <https://doi.org/10.1016/j.jinclphom.2013.01.017>.
- [55] S. Zhu, M.A. Khan, F. Wang, Z. Bano, M. Xia, Exploration of adsorption mechanism of 2-phosphonobutane-1,2,4-tricarboxylic acid onto kaolinite and montmorillonite via batch experiment and theoretical studies, <https://doi.org/10.1016/j.jhazmat.2020.123810>.
- [56] H. Zhang, F. Zhao, M. Xia, F. Wang, Microscopic adsorption mechanism of montmorillonite for common ciprofloxacin emerging contaminant: molecular dynamics simulation and Multiwfnd wave function analysis, <https://doi.org/10.1016/j.colsurfa.2021.126186>.
- [57] M. Othmani, A. Aissa, C.G. Bac, F. Rachdi, M. Debbabi, Surface modification of calcium hydroxyapatite by grafting of etidronic acid, <https://doi.org/10.1016/j.apsurfsci.2013.03.002>.
- [58] S. Saeiabi, K. Achelhi, S. Masse, A. Saeiabi, A. Laghzizil, T. Coradin, Organoapatites for lead removal from aqueous solutions: a comparison between carboxylic acid and aminophosphonate surface modification, <https://doi.org/10.1016/j.colsurfa.2012.12.005>.
- [59] J. Ma, M. Xia, S. Zhu, F. Wang, A new alendronate doped HAP nanomaterial for Pb²⁺, Cu²⁺ and Cd²⁺ effect absorption, <https://doi.org/10.1016/j.jhazmat.2020.123143>.
- [60] M. Zhang, P. Gu, S. Yan, L. Dong, G. Zhang, Na/Zn/Sn/S (NaZTS): Quaternary metal sulfide nanosheets for efficient adsorption of radioactive strontium ions, <https://doi.org/10.1016/j.cej.2019.122227>.
- [61] A. Ivanets, I. Shashkova, N. Kitikova, A. Dzikaya, N. Nekrasova, V. Milyutin, O. Baigenzhenov, K. Zaruba-Venhlinskaya, A. Radkevich, Composite metal phosphates for selective adsorption and immobilization of cesium, strontium, and cobalt radionuclides in ceramic matrices, <https://doi.org/10.1016/j.clepro.2022.134104>.
- [62] M. Zhang, P. Gu, S. Yan, S. Pan, L. Dong, G. Zhang, A novel nanomaterial and its new application for efficient radioactive strontium removal from tap water: KZTS-NS metal sulfide adsorbent versus CTA-F-MF process, <https://doi.org/10.1016/j.chemeng.2020.123486>.
- [63] Y. Yan, X. Dong, X. Sun, X. Sun, J. Li, J. Shen, W. Han, X. Liu, L. Wang, Conversion of waste FGD gypsum into hydroxyapatite for removal of Pb²⁺ and Cd²⁺ from wastewater, <https://doi.org/10.1016/j.jcis.2014.05.010>.
- [64] M. Vila, S. Sánchez-Salcedo, M. Cíciuénez, I. Izquierdo-Barba, M. Vallet-Regí, Novel biopolymer-coated hydroxyapatite foams for removing heavy-metals from polluted water, <https://doi.org/10.1016/j.jhazmat.2011.04.100>.
- [65] F.Y. Wang, H. Wang, J.W. Ma, Adsorption of cadmium (II) ions from aqueous solution by a new low-cost adsorbent—Bamboo charcoal, <https://doi.org/10.1016/j.jhazmat.2009.12.032>.
- [66] Y. Bian, Z. Bian, J. Zhang, A. Ding, S. Liu, L. Zheng, H. Wang, Adsorption of cadmium ions from aqueous solutions by activated carbon with oxygen-containing functional groups, <https://doi.org/10.1016/j.cjche.2015.08.031>.
- [67] S. Wu, K. Zhang, X. Wang, Y. Jia, B. Sun, T. Luo, F. Meng, Z. Jin, D. Lin, W. Shen, L. Kong, J. Liu, Enhanced adsorption of cadmium ions by 3D sulfonated reduced graphene oxide, <https://doi.org/10.1016/j.chemeng.2015.1292-1302>.
- [68] C. Moreno-Castilla, M.A. Álvarez-Merino, M.V. López-Ramón, J. Rivera-Utrilla, Cadmium ion adsorption on different carbon adsorbents from aqueous solutions. Effect of surface chemistry, pore texture, ionic strength, and dissolved natural organic matter, <https://doi.org/10.1021/la049253m>.
- [69] R. Balasubramanian, S.V. Perumal, K. Vijayaraghavan, Equilibrium isotherm studies for the multicomponent adsorption of lead, zinc, and cadmium onto Indonesian peat, <https://doi.org/10.1016/j.indengchemres.2009.2093-2099>.
- [70] M.V. Dinu, E.S. Dragan, A.W. Trochimczuk, Sorption of Pb (II), Cd (II) and Zn (II) by iminodiacetate chelating resins in non-competitive and competitive conditions, <https://doi.org/10.1016/j.desalination.2009.374-379>.

- [71] A.A. Atia, A.M. Donia, A.M. Yousif, Removal of some hazardous heavy metals from aqueous solution using magnetic chelating resin with iminodiacetate functionality, *Sep. Purif. Technol.* 61 (2008) 348–357.
- [72] M.R. Pérez, I. Pavlovic, C. Barriga, J. Cornejo, M.C. Hermosín, M.A. Ulibarri, Uptake of Cu²⁺, Cd²⁺ and Pb²⁺ on Zn-Al layered double hydroxide intercalated with edta, *Appl. Clay Sci.* 32 (2006) 245–251.
- [73] P. Ling, F. Liu, L. Li, X. Jing, B. Yin, K. Chen, A. Li, Adsorption of divalent heavy metal ions onto IDA-chelating resins: simulation of physicochemical structures and elucidation of interaction mechanisms, *Talanta* 81 (2010) 424–432.
- [74] M. Hua, Y. Jiang, B. Wu, B. Pan, X. Zhao, Q. Zhang, Fabrication of a new hydrous Zr (IV) oxide-based nanocomposite for enhanced Pb (II) and Cd (II) removal from waters, *ACS Appl. Mater. Interfaces* 5 (2013) 12135–12142.
- [75] Y. Yan, M. Du, L. Jing, X. Zhang, Q. Li, J. Yang, Green synthesized hydroxyapatite for efficient immobilization of cadmium in weakly alkaline environment, <https://doi.org/10.1016/j.envres.2023.115445>.
- [76] Y. Wang, W. Yao, Q. Wang, Z. Yang, L. Liang, L. Chai, Synthesis of phosphate-embedded calcium alginate beads for Pb(II) and Cd(II) sorption and immobilization in aqueous solutions, <https://doi.org/10.1016/j.tnnf.2016.06.001>, *Trans. Nonferrous Met. Soc. China* 26 (2016) 2230–2237, [https://doi.org/10.1016/S1003-6326\(16\)64340-6](https://doi.org/10.1016/S1003-6326(16)64340-6).
- [77] F. Wang, P. Wu, L. Shu, Di Huang, H. Liu, High-efficiency adsorption of Cd(II) and Co(II) by ethylenediaminetetraacetic dianhydride-modified orange peel as a novel synthesized adsorbent, <https://doi.org/10.1016/j.espol.2022.25748-25758>, <https://doi.org/10.1007/s11356-021-17501-7>.
- [78] F. Fang, L. Kong, J. Huang, S. Wu, K. Zhang, X. Wang, B. Sun, Z. Jin, J. Wang, X.-J. Huang, Removal of cobalt ions from aqueous solution by an amination graphene oxide nanocomposite, *J. Hazard. Mater.* 270 (2014) 1–10.
- [79] S. Hashemian, H. Saffari, S. Ragabion, Adsorption of cobalt (II) from aqueous solutions by Fe 3 O 4/bentonite nanocomposite, *Water, Air, Soil Pollut.* 226 (2015) 1–10.
- [80] Y. Asci, S. Kaya, Removal of cobalt ions from water by ion-exchange method, *DESLIMINATION WATER Treat.* 52 (2014) 267–273.
- [81] P.N. Nomngongo, J.C. Ngila, T.A.M. Msagati, B. Moodley, Kinetics and equilibrium studies for the removal of cobalt, manganese, and silver in ethanol using Dowex 50W-x8 cation exchange resin, *Sep. Sci. Technol.* 49 (2014) 1848–1859.
- [82] M. Ansari, A. Raisi, A. Aroujalian, B. Dabir, M. Irani, Synthesis of nano-NaX zeolite by microwave heating method for removal of lead, copper, and cobalt ions from aqueous solution, *J. Environ. Eng.* 141 (2015) 4014088.
- [83] H. Wang, H. Tang, Z. Liu, X. Zhang, Z. Hao, Z. Liu, Removal of cobalt (II) ion from aqueous solution by chitosan–montmorillonite, *J. Environ. Sci.* 26 (2014) 1879–1884.
- [84] M. Ferri, S. Campisi, A. Gervasini, Nickel and cobalt adsorption on hydroxyapatite: a study for the de-metalation of electronic industrial wastewaters, <https://doi.org/10.1016/j.adsorp.2019.06.001>, *Adsorption* 25 (2019) 649–660, <https://doi.org/10.1007/s10450-019-00066-w>.
- [85] T.N. Tran, J. Kim, J.-S. Park, Y. Chung, J. Han, S. Oh, S. Kang, Novel hydroxyapatite beads for the adsorption of radionuclides from decommissioned nuclear power plant sites, <https://doi.org/10.1016/j.applsci.2021.1746>, <https://doi.org/10.3390/app11041746>.
- [86] R. Foroutan, S.J. Peighambardoust, A. Ahmadi, A. Akbari, S. Farjadfar, B. Ramavandi, Adsorption mercury, cobalt, and nickel with a reclaimable and magnetic composite of hydroxyapatite/Fe3O4/polydopamine, <https://doi.org/10.1016/j.jechemeng.2021.105709>, <https://doi.org/10.3390/app11041746>.
- [87] A.A. Alqadami, M.A. Khan, M. Otero, M.R. Siddiqui, B.-H. Jeon, K.M. Batoo, A magnetic nanocomposite produced from camel bones for an efficient adsorption of toxic metals from water, <https://doi.org/10.1016/j.jcleanprod.2018.01.023>.
- [88] A.A. Alqadami, M. Naushad, M.A. Abdalla, T. Ahamad, Z. Abdullah Alothman, S. M. Alshehri, A.A. Ghfar, Efficient removal of toxic metal ions from wastewater using a recyclable nanocomposite: a study of adsorption parameters and interaction mechanism, <https://doi.org/10.1016/j.jcleanprod.2017.04.085>.
- [89] K. Lu, Z. Zhao, J. Cui, C. Bai, H. Zhang, X. Zhao, F. Wang, M. Xia, Y. Zhang, The immobilization of Sr(II) and Co(II) via magnetic easy-separation organophosphonate-hydroxyapatite hybrid nanoparticles, <https://doi.org/10.1016/j.seppur.2023.123750>.
- [90] S. Zhu, M. Asim Khan, F. Wang, Z. Bano, M. Xia, Rapid removal of toxic metals Cu²⁺ and Pb²⁺ by amino trimethylene phosphonic acid intercalated layered double hydroxide: a combined experimental and DFT study, <https://doi.org/10.1016/j.chemeng.2020.123711>, <https://doi.org/10.1016/j.cej.2019.123711>.
- [91] X. Fang, S. Zhu, J. Ma, F. Wang, H. Xu, M. Xia, The facile synthesis of zoledronate functionalized hydroxyapatite amorphous hybrid nanobiomaterial and its excellent removal performance on Pb²⁺ and Cu²⁺, <https://doi.org/10.1016/j.jhazmat.2020.122291>.
- [92] J. Zhang, X. Li, H. Xu, W. Zhang, X. Feng, Y. Yao, Y. Ma, L. Su, S. Ren, S. Li, Removal of Cd²⁺, Pb²⁺ and Ni²⁺ from water by adsorption onto magnetic composites prepared using humic acid from waste biomass, <https://doi.org/10.1016/j.jcleanprod.2023.137237>.
- [93] A.A. Alqadami, M. Naushad, M.A. Abdalla, T. Ahamad, Z. Abdullah Alothman, S. M. Alshehri, A.A. Ghfar, Efficient removal of toxic metal ions from wastewater using a recyclable nanocomposite: a study of adsorption parameters and interaction mechanism, <https://doi.org/10.1016/j.jcleanprod.2017.04.085>.
- [94] J.L. Casals-Sainz, A. Fernandez-Alarcon, E. Francisco, A. Costales, A. Martin Pendas, Bond order densities in real space, <https://doi.org/10.1021/acs.jpcsa.9b10113>.
- [95] M. Menéndez, R. Álvarez Boto, E. Francisco, P.A. Martín, One-electron images in real space: natural adaptive orbitals, *J. Comput. Chem.* 36 (2015) 833–843.